Origin of premature fracture and enhancement of superelasticity in laser additively manufactured Ni-rich NiTi metamaterials

Yan, Zhaorui; Zhu, Jia Ning; Yang, Yi Chieh; Brouwer, Hans; Riemslag, Ton; Jinschek, Joerg R.; Hermans, Marcel; Jovanova, Jovana; Popovich, Vera

DOI
10.1016/j.scriptamat.2025.116558

Publication date
2025

Document Version
Final published version

Published in
Scripta Materialia

Scripta Materialia 259 (2025) 116558

Contents lists available at ScienceDirect

Scripta Materialia

journal homepage: www.journals.elsevier.com/scripta-materialia

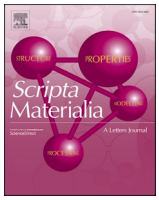

Origin of premature fracture and enhancement of superelasticity in laser additively manufactured Ni-rich NiTi metamaterials

Zhaorui Yan [a], Jia-Ning Zhu [a,*], Yi-Chieh Yang [b], Hans Brouwer [a], Ton Riemslag [a], Joerg R. Jinschek [b], Marcel Hermans [a], Jovana Jovanova [a], Vera Popovich [a,*]

[a] Faculty of Mechanical Engineering, Delft University of Technology, Mekelweg 2, 2628 CD, Delft, the Netherlands
[b] National Center for Nano Fabrication and Characterization (DTU Nanolab), Technical University of Denmark (DTU), Kgs. Lyngby, Denmark

ARTICLE INFO

Keywords:
NiTi
Shape memory alloys
Superelasticity
Metamaterials
Additive manufacturing

ABSTRACT

Superelastic metamaterials have attracted significant attention recently, but achieving such functionality remains challenging due to partial superelasticity and premature fracture in additively manufactured components. To address these issues, this study investigates the premature fracture in Ni-rich NiTi metamaterials fabricated by laser powder bed fusion. A comparative analysis of two structures (Gyroid network and Diamond shell) reveals that the structural stability of bending- and stretching-dominated structures is reversed compared to typical elastic-plastic response, due to the tension-compression asymmetry of base NiTi. The premature fracture and partial superelasticity of these as-fabricated samples are attributed to low deformation ability for accommodating tensile stress. Based on these findings, a heat treatment introducing Ni_4Ti_3 precipitates was employed, successfully achieving macroscopic superelasticity in the NiTi metamaterials, with consistency between model prediction and experiments.

In recent years, the rapid development of additive manufacturing (AM) of Nitinol (NiTi) has transitioned production from bulk materials to customized structures and metamaterials. Due to the deformation recoverability of NiTi alloys, NiTi metamaterials have shown wide applications such as shock absorption, bio-implants, and actuators [1–4]. Deformation recoverability in most cases of NiTi metamaterials only relies on the shape memory effect, rather than superelasticity [5–8]. This requires external stimuli for activation of shape recovery. However, spontaneous deformation recoverability of metallic metamaterials is more desirable across different industrial sectors [9–11]. Researchers have attempted to manufacture superelastic metamaterials using Ni-rich NiTi alloys, but only partial superelasticity has been achieved due to the low recoverability and premature fracture [12,13]. In our previous study, broad scatter in deformation recoverability within the investigated structure has been observed, which results from variations in compositional and microstructural distribution. This is the main cause for the low deformation recoverability during uniaxial compression of NiTi metamaterials [14]. Thus, this study focuses on the fracture mechanisms of Ni-rich NiTi metamaterials fabricated using laser powder bed fusion (L-PBF) and further provides a solution for enhancing superelasticity in NiTi metamaterials.

The macroscopic properties of NiTi metamaterials are influenced by the interaction between the NiTi functionalities and the structural stiffness [12,15]. The former, including shape memory effect and superelasticity, originated from reversible martensitic transformation. The reversible martensitic transformation is sensitive to the local microstructure and compositions. The structural stiffness is determined by the unit cell structure and the relative density [16]. This relationship between microstructure, mesoscale deformation, and macroscopic response indicates that the premature fracture mechanism could be considered as material-related or structure-related.

Based on the structure-stiffness relationship in mechanical metamaterials, the deformation modes are categorized into two types: bending-dominated and stretching-dominated behaviors [17–19]. By generalizing the Gibson-Ashby theory to martensitic transformation, bending-dominated structures exhibit high deformation recoverability due to their structural compliance [12,15,20]. The complete classification of triply periodic minimal surface (TPMS)-type structures as either bending- or stretching-dominated is still under discussion [21]. However, two typical TPMS-type designs were chosen: Diamond shell structure, which exhibits typical stretching-dominated behavior, and the Gyroid network structure, which is typically bending-dominated

* Corresponding authors.
E-mail addresses: J.zhu-2@tudelft.nl (J.-N. Zhu), V.Popovich@tudelft.nl (V. Popovich).

https://doi.org/10.1016/j.scriptamat.2025.116558
Received 8 November 2024; Received in revised form 9 January 2025; Accepted 10 January 2025
Available online 16 January 2025

[22–24]. The rationale behind this choice is to investigate whether the premature fracture observed Ni-rich NiTi structure is related to the structure configuration, as premature fracture is not observed in bulk samples when the same process parameters are used in the manufacturing of all samples [12].

Numerous studies have investigated the fracture behaviors of superelastic NiTi alloys produced through conventional manufacturing methods [25–28]. However, the failure criteria and fracture mechanisms of additively manufactured NiTi base materials under various loading directions and stress states remain unclear. Failure theories, such as the von Mises and Johnson-Cook criteria, which are commonly applied to metallic metamaterials made from ductile metals, are not reasonably applicable to the modeling of NiTi structures [29,30]. Therefore, the fracture mechanism of NiTi metamaterials has yet to be explained [14].

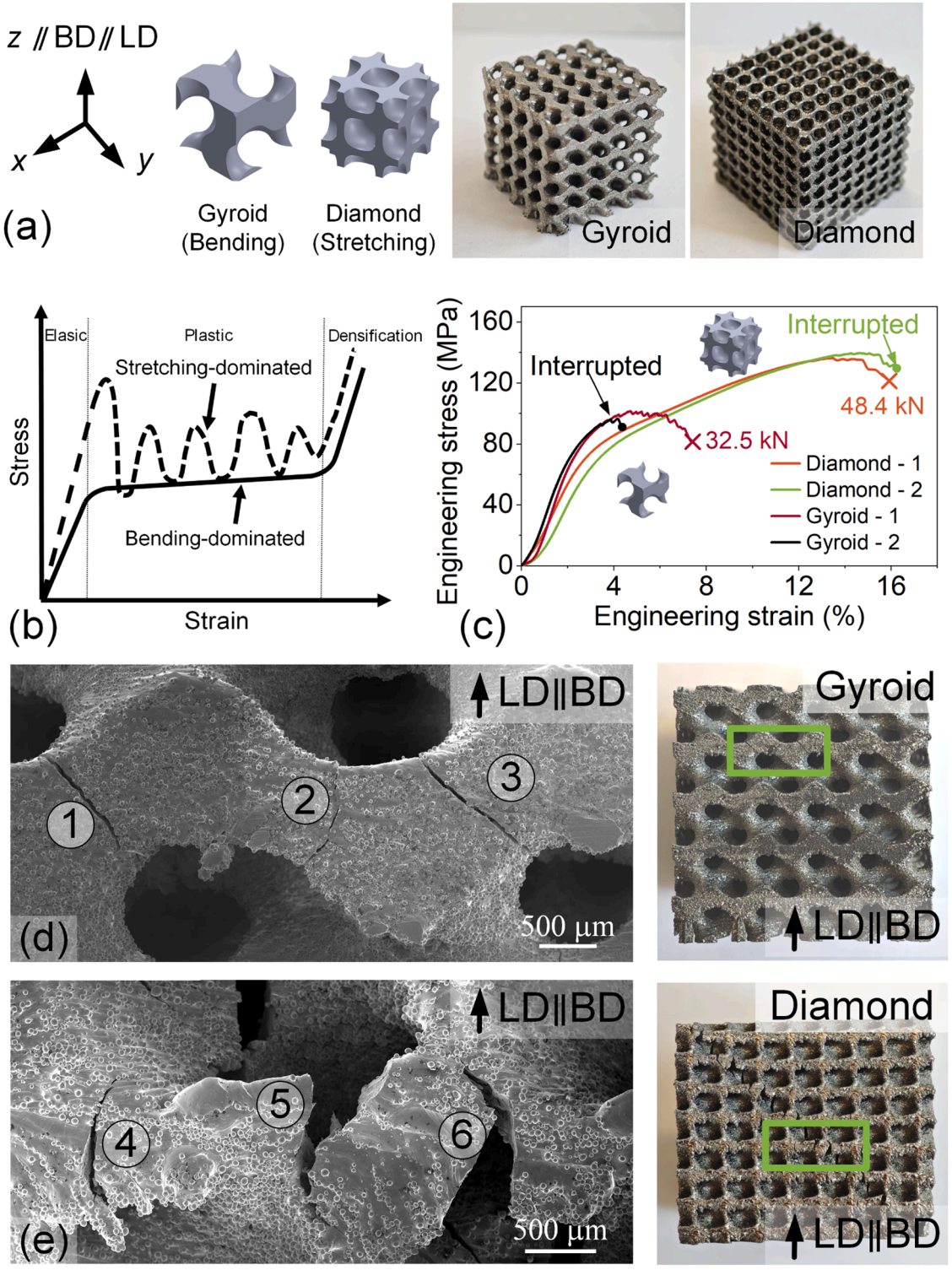

Fig. 1. (a) Geometric model and as-fabricated samples; (b) Schematic diagram of bending-dominated and stretching-dominated behavior of ductile metallic metamaterials, reproduced from [22,36]; (c) Engineering stress-strain curves of Gyroid and Diamond samples under uniaxial compression from fracture tests; (c) Profiles of interrupted samples; and crack formation in (d) Gyroid network and (e) Diamond shell structures and the selected area are marked by green rectangular box.

In this study, the premature fracture mechanisms in superelastic NiTi metamaterials have been investigated. The geometries of the Gyroid and Diamond surfaces are described using the level-set functions [31]. A unit cell size of 5 mm and a configuration of 4 × 4 × 4 (64) unit cells are used for the periodicity. The Diamond shell structure was generated by thickening a surface into a shell structure with a nominal relative density of 0.25. The Gyroid network structure was modeled by dividing the solid volume using a single surface, for a nominal relative density of 0.3 (Fig. 1(a)). A material model developed by Auricchio et al. was used for numerical computations [32,33]. In this model, the increment of total strain $\Delta\varepsilon$ is defined as the sum of elastic strain increment $\Delta\boldsymbol{\varepsilon}^{\mathrm{el}}$ and the increment of equivalent transformation strain $\Delta\boldsymbol{\varepsilon}^{\mathrm{tr}}$:

$$\Delta\boldsymbol{\varepsilon} = \Delta\boldsymbol{\varepsilon}^{\mathrm{el}} + \Delta\boldsymbol{\varepsilon}^{\mathrm{tr}}. \tag{1}$$

The increment of equivalent transformation strain of NiTi is defined by:

$$\Delta\boldsymbol{\varepsilon}^{\mathrm{tr}} = \Delta\xi\frac{\partial G^{\mathrm{tr}}}{\partial\boldsymbol{\sigma}}, \tag{2}$$

where G^{t} is the transformation potential, ξ the volume fraction of martensite phase, and $\boldsymbol{\sigma}$ the Cauchy stress tensor. The transformation potential refers to the potential function used to describe inelastic deformation during martensitic phase transformation. The tetrahedral mesh with an average size of 0.12 mm was used. The numerical samples were compressed between two rigid planes, with the upper plane moving downward by 0.066 mm and a friction coefficient of 0.2 assumed for all contacts. The numerical solution was performed using Abaqus/Explicit 2019, with semi-automatic mass scaling targeting 2.5 million steps after monitoring kinetic energy (details in Figs. S1-S2 and Tables S1-S2).

Samples were fabricated using laser powder bed fusion (Aconity 3D Midi) from $Ni_{51.4}Ti_{48.6}$ powder prepared by gas atomization in a high-purity argon-filled chamber (Fig. 1(a)). Process parameters used in this study include a laser power of 400 W, scanning speed of 1250 mm/s, hatch distance of 0.120 mm, layer thickness of 0.030 mm, and a stripe scanning strategy with a 67.5° rotation [34]. Following printing, heat treatment includes solution annealed at 950 °C for 60 min followed by air cooling for 20 min, aging treatment at 450 °C for 90 min followed by air cooling to room temperature. All samples were sealed in vacuum quartz ampoules to prevent oxidation during heat treatment.

A quasi-static tensile test was performed on mini-scaled dogbone samples using a contact extensometer with a 7 mm gauge length (Fig. S3). Cyclic tension tests included 15 cycles with a maximum displacement of 0.22 mm. Quasi-static compression tests were carried out on Gyroid and Diamond structures using a contact extensometer using a contact extensometer with a maximum displacement of 4.4 mm. The samples were quasi-statically compressed until complete structural failure. All uniaxial tests were conducted on a Zwick 100 mechanical testing platform at 54 °C with a strain rate of 2×10^{-4} s^{-1}. The transformation temperatures of these samples are shown in Fig. S4.

Fracture analysis was performed using a Scanning Electron Microscope (JSM-IT100) on samples from uniaxial compression tests. EBSD samples were prepared using electropolishing (Struers LectroPol5) on the macroscopic (100) cross-section aligned with the building direction (BD). Texture analysis was conducted using a scanning electron microscope (SEM) equipped with an electron backscatter diffraction (EBSD) detector (Helios G4) with a step size of 1.5 μm. Characterization using both bright-field transmission electron microscopy (TEM) TEM and scanning transmission electron microscopy (STEM) was conducted with spherical aberration-corrected transmission electron microscopes at an accelerating voltage of 300 kV. TEM experiments utilized an image-corrected Titan TEM 80–300 (Thermo Fisher Scientific Inc.) with a OneView camera (Gatan Inc.). STEM and EDS experiments were performed with a Spectra 300 S/TEM (Thermo Fisher Scientific Inc.), equipped with high-angle annular dark field (HAADF) and an Ultra-X EDS detector. For the STEM experiment, a probe semi-convergence angle of 28.7 mrad and a camera length of 342 mm were used.

Compressive fracture tests were conducted on the as-fabricated samples (Fig. 1(a)) with loading direction (LD) aligned with the building direction (BD) at a temperature of 54 °C. The engineering stress-strain curves from fracture tests are compared in Fig. 1(c) and Fig. S5. The engineering stress-strain curves show a reversed trend compared to the deformation behavior of metamaterials made from ductile metals (Fig. 1(b)) [18,22,35]. Diamond shell structures, which are stretching-dominated, exhibit an increasing effective stress and plateau-like response after initial elasticity. The Gyroid network structure shows typical elastic-brittle behavior [17]. The stress oscillates after the elasticity stage and the deformation mode is brittle fracture. The initial damage strain of the Gyroid structure is 3.7 %, with a collapse strain of 7.3 %. In contrast, the Diamond structure exhibits an initial damage strain of 12.5 % and a collapse strain of 15.9 %. The stability of the stretching-dominated Diamond structure makes it more attractive for load bearing applications. This reversed trend in large deformation compression implies a need for a reexamination of the constitutive NiTi behaviors.

Generally, the fracture of mechanical metamaterials involves the formation and propagation of cracks. To analyze the premature fracture, experiments were interrupted before the final collapse of the structures (Fig. 1(c)). The SEM images of crack initiation and propagation are shown in Fig. 1(d) and (e). The crack formation exhibits a repeated pattern in different unit cells (Fig. S6 and S7). In the Gyroid network unit cell, two discrete crack formations are observed (Fig. 1(d) ② ③), while three discrete crack initiations are observed in the Diamond structure (Fig. 1(e) ③ ④ ⑤).

For these reversed phenomena from uniaxial compression, our hypothesis is that the tension-compression asymmetry of base NiTi leads to the premature failure of the as-fabricated structures. The asymmetric behavior between tension and compression in the as-fabricated bulk samples is compared in Fig. 2(a). Using the same parameters for manufacturing bulk samples, the compressive sample demonstrates stress-induced martensitic transformation at 54 °C [12]. In the initial cycle, it shows significant compressive deformation capacity with a maximum strain of 8.3 %. In cycle 15, the bulk sample exhibits a maximum strain of 5.7 % and a transformation strain of 3.7 %. In contrast, the tensile sample only achieves a maximum strain of 4.0 %, which is the best data in repeating tests. Cyclic tension tests reveal suppressed superelasticity, characterized by a recoverable strain of 1.75 % and a narrow hysteresis area. Recent studies have demonstrated that Ni-rich NiTi with compressive superelasticity can be achieved across a broad process window, but the process window for tensile superelasticity is more limited [37,38]. For tensile superelasticity, careful adjustment of Ni concentration and texture [39,40], or improvements through heat treatment promoting Ni_4Ti_3 precipitation [41], are required. The suppressed tensile superelasticity observed in our as-fabricated samples is consistent with the above findings.

To test our hypothesis, the maximum principal stresses for these structures are illustrated in Fig. 2(b), with a colormap indicating compressive and tensile principal strain. Under uniaxial compression along the macroscopic [100] direction, the Gyroid network structure, due to its bending-dominated behavior and non-slender geometry, exhibits high tensile principal strain. In contrast, the Diamond shell structure is less sensitive to tensile strain under the same loading conditions. Fig. 2(c) shows the equivalent transformation strains for the Gyroid and Diamond structures. In the Gyroid structure, transformation localization forms in both compressive and tensile areas, but these transformation regions remain isolated. In the Diamond shell structure, martensitic transformations are interconnected along the compressive loading direction. By comparing the interrupted experiments (Fig. 1(c) (d)) and numerical results Fig. 2(b), the observed crack initiations in both structures correspond to areas of concentrated tensile stress. Therefore, the cracks at the millimeter scale in both structures are initiated from tensile stress areas. Under uniaxial compression with the

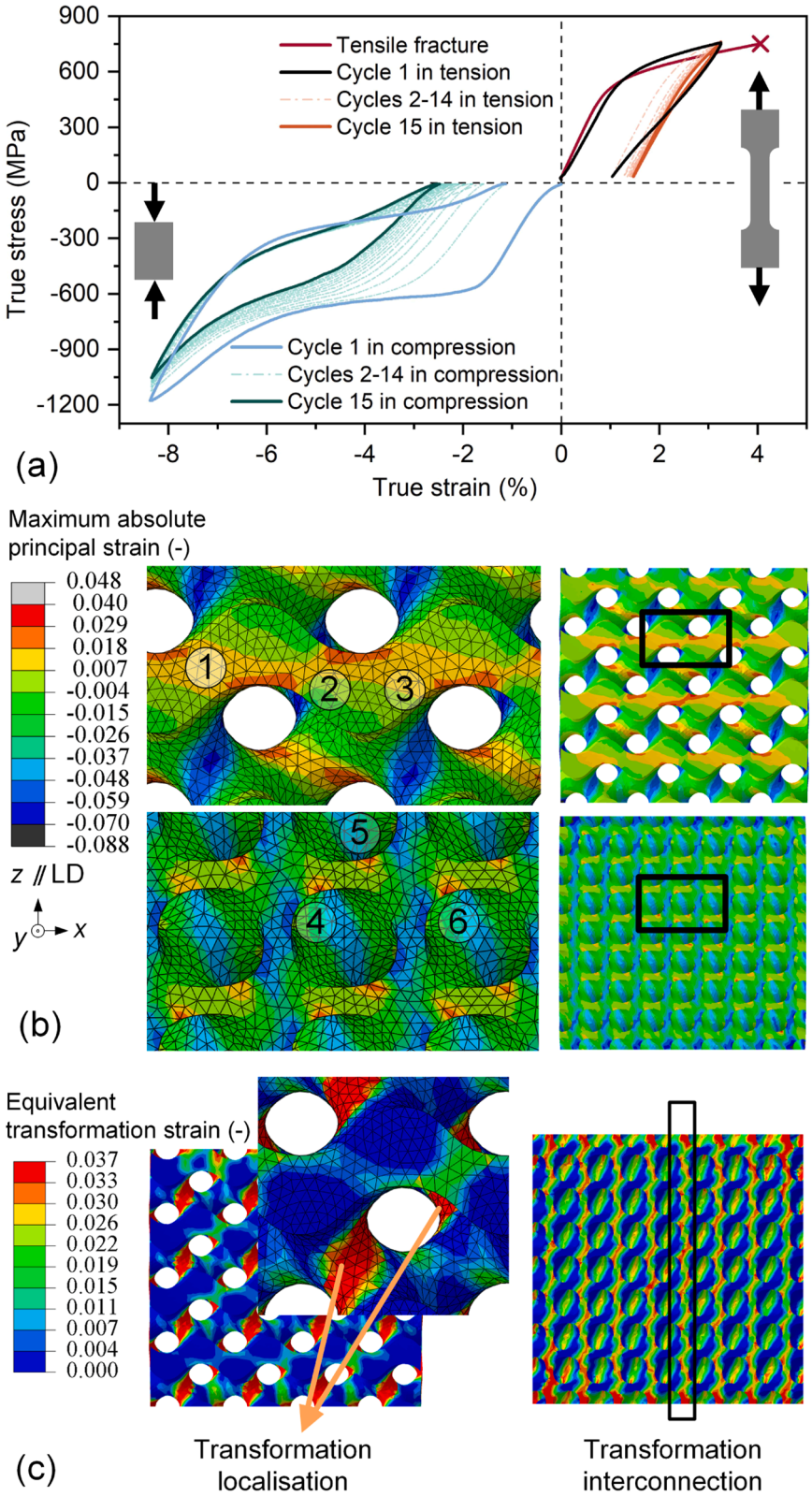

Fig. 2. (a) Tension-compression asymmetry of base NiTi; (b) Maximum absolute principal strain; (c) Equivalent transformation strain of the Gyroid and Diamond structures under uniaxial compression at maximum loading.

same macroscopic loading, the Gyroid structure is more susceptible to crack initiation due to the tensile sensitivity of bending-dominated behavior.

From a macroscopic view in Fig. 3, both structures exhibit final failure along a shear band on the macroscopic {110} plane. Clear brittle fracture characteristics are observed as shown in Fig. 3(a) and (b). At high magnification of river-like patterns, some dimples were observed, suggesting ductile damage during crack propagation. However, the size and distribution of these micro-dimples suggest that ductile damage was not the dominant mechanism [27].

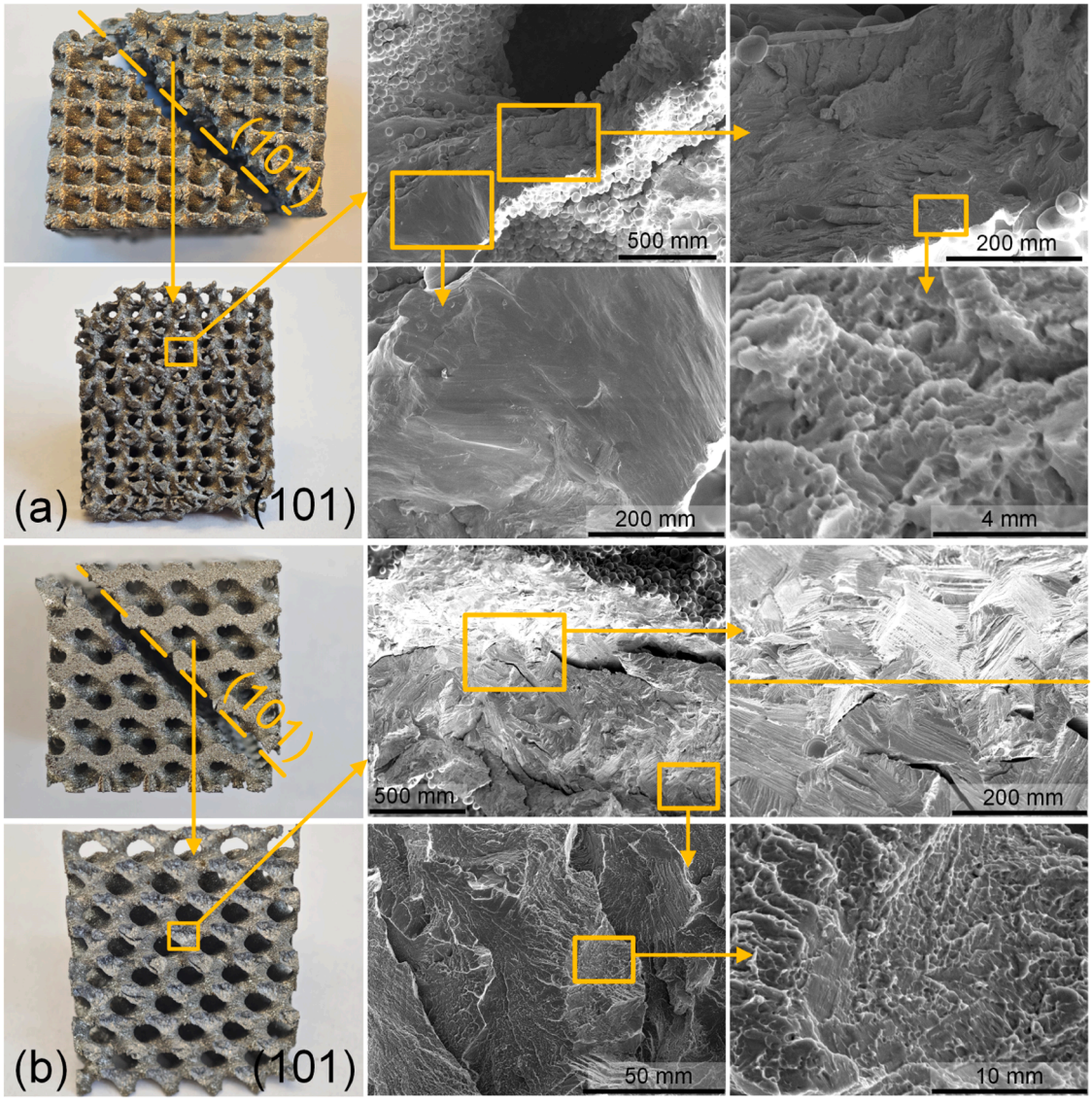

Fig. 3. Fracture surface of (a) Gyroid and (b) Diamond structures.

The formation of the macroscopic {110} fracture surface and the associated brittle fracture characteristics differ from the shear bands typically observed in ductile bulk materials [42]. In NiTi structures, brittle fracture is primarily driven by strain localization and mesoscopic deformation. In the Diamond shell structure, continuous fracture surfaces occur along the macroscopic {110} planes, with two distinct regions in Fig. 3(b): cleavage river patterns and tearing ridges in the tensile area, and a smooth shearing plane. Cracks initiate in the tensile region due to strain localization. Upon losing stability, the entire structure collapses along the continuous shearing plane under a compressive force of 48.4 kN [22,23]. In the Gyroid structure, the zoomed-in area reveals two intersecting fracture surfaces. Cracks form in the tensile region and the rapid propagation of them creates intersecting fracture planes. The interconnection of the fracture planes causes the final {110} fracture plane and structural failure under a compressive force of 32.5 kN.

The EBSD characterization on the macroscopic (100) plane||BD of the Diamond shell structure and Gyroid network structure is shown in Fig. 4 (a), with a colormap corresponding to BD in the inverse pole figure (IPF). Since the slip system for the B2 phase is {110}<001>, the Taylor factors with loading direction along the building direction are plotted in Fig. 4(b) and (f). In the Diamond shell structure, grains with smaller Taylor factors are primarily presented near the edges, as shown in the extracted grains (Fig. 4(g)). This leads to unstable deformation near the edges, consistent with the simulated results where tensile stress is concentrated in these areas.

The effective properties of mechanical metamaterials are defined under assumptions of homogeneity and tension-compression symmetry in the base NiTi [12]. However, experimental results reveal that the tension-compression asymmetry of base NiTi reverses the structural stability of the two structures. To evaluate the deformation capacity driven by reversible martensitic transformation, the structures were chosen to minimize structural compliance (Fig. S1). This ensured that the macroscopic deformation primarily originated from the base NiTi rather than the elastic deformation of the compliant structure. In tensile regions, large deformations of base NiTi cannot be achieved through either the initiation of martensitic transformation or the limited dislocation slip system.

Microstructural inhomogeneity [14,43], and premature fracture have been identified as challenges for the engineering application of NiTi metamaterials and structures. To simultaneously mitigate these issues, we have employed heat treatment to enhance the superelasticity by introducing Ni_4Ti_3 precipitates in the Diamond shell structure. Homogenization followed by aging is applied to release residual stress,

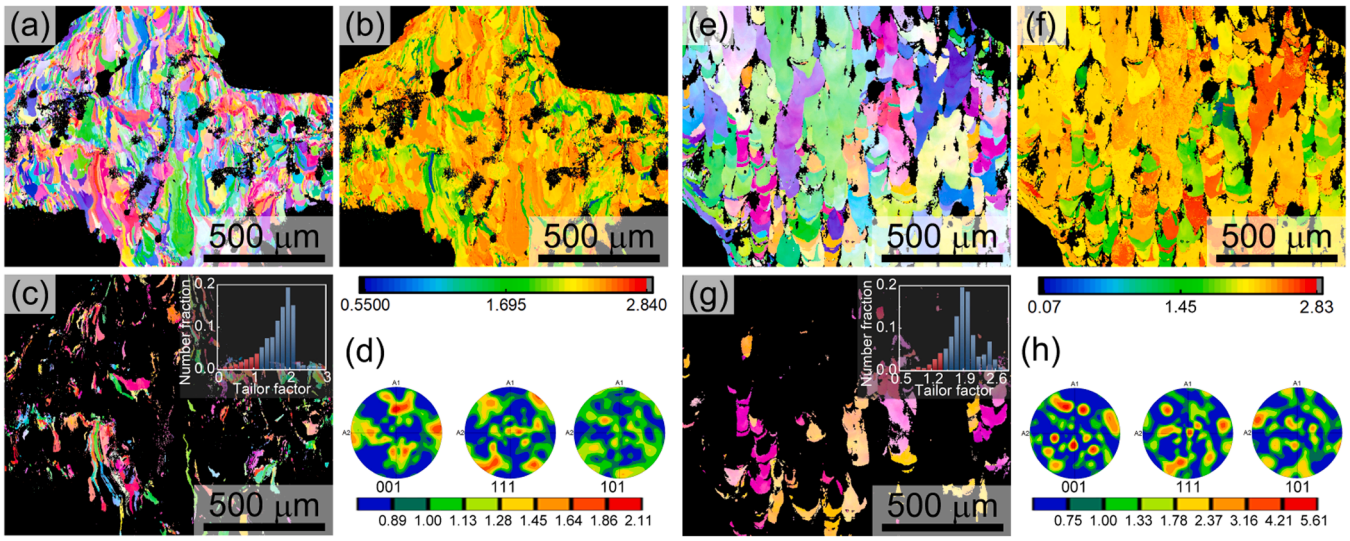

Fig. 4. EBSD inverse pole figure (IPF) maps with pole figures: (a) Diamond shell and (e) Gyroid network; Taylor factors for (b) Diamond shell and (f) Gyroid network; extracted grains with low Taylor factor values highlighted in red for (c) Diamond shell and (g) Gyroid network; and pole figure for (d) Diamond shell and (h) Gyroid network, with sample direction corresponding to the building direction.

homogenize microstructure and introduce Ni_4Ti_3 precipitates. As shown in Fig. 5(a) and (b), the as-fabricated Diamond samples has a higher critical stress for stress-induced transformation (~65 MPa) compared to the heat-treated samples (~50 MPa). This difference can be attributed to the precipitation of Ni_4Ti_3 (Fig. 5(e)), which reduces the Ni content in the NiTi matrix and decreases the critical stress required for transformation [44]. The heat-treated NiTi also shows a higher hardening rate beyond 4.5 % strain and a greater recoverable strain (72 %) than the as-fabricated sample (35 %), both suggest that Ni_4Ti_3 precipitates play a key role [41,45]: Enhancing dislocation slip resistance in both the austenite and stress-induced martensite phases, preventing plastic deformation even at higher stress levels (180 MPa). This enhanced slip resistance contributes to the superior superelasticity of the heat-treated NiTi. In contrast, the as-fabricated NiTi, lacking sufficient precipitation strengthening (Fig. 5(d)), cannot maintain stress-induced martensitic transformation alone with increasing strain and is accompanied by plastic deformation, resulting in a lower hardening rate when the strain exceeds 4.5 %. To the best of the authors' knowledge, this is the first time that model-experiment consistency in superelastic response is reported in AM superelastic metamaterials, as mechanical metamaterials were initially defined as materials designed through mechanically homogenized models. Moreover, the premature fracture in Gyroid network

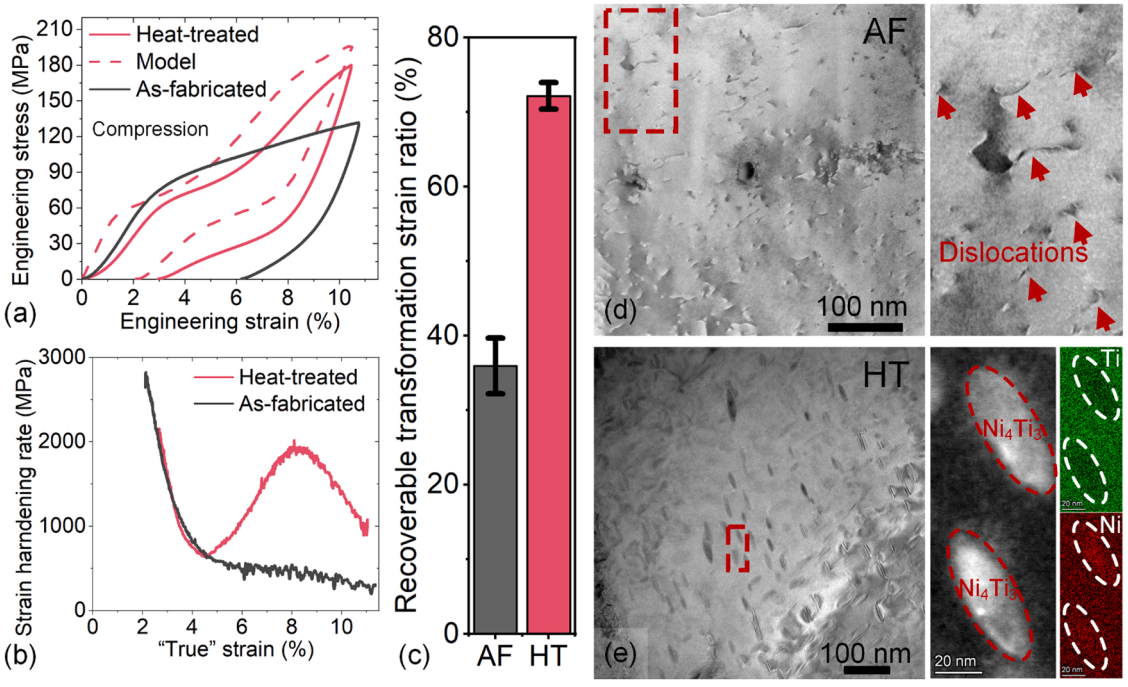

Fig. 5. (a) Engineering stress-strain curves under uniaxial compression, (b) strain hardening rates during loading, (c) recoverable transformation strain ratios for as-fabricated (AF) and heat-treated (HT) Diamond shell structured NiTi; (d) bright-field transmission electron microscope (TEM) images showing dislocations in as-fabricated sample and (e) TEM images along with scanning transmission electron microscope (STEM) images and energy-dispersive X-ray spectra (STEM-EDS) showing Ni_4Ti_3 precipitates in heat-treated sample.

structures was mitigated (Fig. S8).

In summary, this study shows that the premature fracture of Ni-rich NiTi metamaterials originates from the low deformation ability of base material to accommodate the tensile stress. The tension-compression asymmetry changes the structural stability of bending- and stretching-dominated structures. For the first time, we achieved model-experiment consistency in superelastic metamaterials with a recoverable plateau-like response and second hardening. The heat treatment following L-PBF is crucial for microstructural homogenization and introducing Ni_4Ti_3 precipitates in Ni-rich NiTi metamaterials.

Declaration of generative AI and AI-assisted technologies in the writing process

During the preparation of this work the authors used ChatGPT in order to assist with grammar improvement. After using this tool, the authors reviewed and edited the content as needed and take full responsibility for the content of the publication.

CRediT authorship contribution statement

Zhaorui Yan: Writing – original draft, Methodology, Investigation, Formal analysis, Conceptualization. **Jia-Ning Zhu:** Writing – review & editing, Investigation, Formal analysis. **Yi-Chieh Yang:** Investigation, Formal analysis. **Hans Brouwer:** Methodology, Investigation. **Ton Riemslag:** Methodology, Investigation. **Joerg R. Jinschek:** Writing – review & editing, Supervision. **Marcel Hermans:** Writing – review & editing, Supervision. **Jovana Jovanova:** Supervision. **Vera Popovich:** Writing – review & editing, Supervision.

Declaration of interests

The authors declare that they have no known competing financial interests or personal relationships that could have appeared to influence the work reported in this paper.

Acknowledgement

The authors are grateful to Evgenii Borisov (from Peter the Great Saint-Petersburg Polytechnic University) for support in the additive manufacturing. The authors also would like to acknowledge Raymond Dekker, Elise Reinton, Durga Mainali, and Kees Kwakernaak, for their help with the heat treatment, materials characterization, and mechanical tests.

Supplementary materials

Supplementary material associated with this article can be found, in the online version, at doi:10.1016/j.scriptamat.2025.116558.

References

[1] M. Elahinia, N. Shayesteh Moghaddam, M. Taheri Andani, A. Amerinatanzi, B. A. Bimber, R.F. Hamilton, Fabrication of NiTi through additive manufacturing: a review, Prog. Mater. Sci. 83 (2016) 630–663.
[2] Z.G. Karaji, M. Speirs, S. Dadbakhsh, J.P. Kruth, H. Weinans, A.A. Zadpoor, S. A. Yavari, Additively manufactured and surface biofunctionalized porous nitinol, ACS Appl. Mater. Interf. 9 (2017) 1293–1304.
[3] V. Finazzi, F. Berti, L. Petrini, B. Previtali, A.G. Demir, Additive manufacturing and post-processing of superelastic NiTi micro struts as building blocks for cardiovascular stents, Addit. Manuf. 70 (2023) 103561.
[4] G. Liu, X. Zhang, X. Chen, Y. He, L. Cheng, M. Huo, J. Yin, F. Hao, S. Chen, P. Wang, S. Yi, L. Wan, Z. Mao, Z. Chen, X. Wang, Z. Cao, J. Lu, Additive manufacturing of structural materials, Mater. Sci. Eng. R Rep. 145 (2021) 100596.
[5] Z. Xiong, M. Li, S. Hao, Y. Liu, L. Cui, H. Yang, C. Cui, D. Jiang, Y. Yang, H. Lei, Y. Zhang, Y. Ren, X. Zhang, J. Li, 3D-printing damage-tolerant architected metallic materials with shape recoverability via special deformation design of constituent material, ACS Appl. Mater. Interf. 13 (2021) 39915–39924.
[6] X. Li, H. Wang, L. Sun, X. Wang, Y. Pan, M. Zhou, X. Guo, 3D chiral energy-absorbing structures with a high deformation recovery ratio fabricated via selective laser melting of the NiTi alloy, ACS Appl. Mater. Interf. (2023) 53746–53754.
[7] Q. Liu, S. Ghodrat, K.M.B. Jansen, Design and modelling of a reversible shape memory alloy torsion hinge actuator, Mater. Des. 237 (2024) 112590.
[8] Y. Yang, Y. Wang, Snapping for 4D-printed insect-scale metal-jumper, Adv. Sci. 2307088 (2023) 1–10.
[9] N.B. Morgan, Medical shape memory alloy applications - The market and its products, Mater. Sci. Eng. A 378 (2004) 16–23.
[10] J. Van Humbeeck, Non-medical applications of shape memory alloys, Mater. Sci. Eng. A 273–275 (1999) 134–148.
[11] J. Mohd Jani, M. Leary, A. Subic, M.A. Gibson, A review of shape memory alloy research, applications and opportunities, Mater. Des. 56 (2014) 1078–1113.
[12] Z. Yan, J. Zhu, E. Borisov, T. Riemslag, S. Paul, M. Hermans, J. Jovanova, V. Popovich, Superelastic response and damping behavior of additively manufactured Nitinol architectured materials, Addit. Manuf. 68 (2023) 103505.
[13] S. Dadbakhsh, M. Speirs, J.P. Kruth, J. Van Humbeeck, Influence of SLM on shape memory and compression behaviour of NiTi scaffolds, CIRP Ann. - Manuf. Technol. 64 (2015) 209–212.
[14] Z. Yan, J.N. Zhu, D. Hartl, T. Riemslag, S.P. Scott, R. Petrov, M. Hermans, J. Jovanova, V. Popovich, Correlation between microstructural inhomogeneity and architectural design in additively manufactured NiTi shape memory alloys, Virtual Phys. Prototyp. 19 (2024) 1–20.
[15] P.A. Michailidis, N. Triantafyllidis, J.A. Shaw, D.S. Grummon, Superelasticity and stability of a shape memory alloy hexagonal honeycomb under in-plane compression, Int. J. Solids Struct. 46 (2009) 2724–2738.
[16] X. Yu, J. Zhou, H. Liang, Z. Jiang, L. Wu, Mechanical metamaterials associated with stiffness, rigidity and compressibility: a brief review, Prog. Mater. Sci. 94 (2018) 114–173.
[17] L.J. Gibson, M.F. Ashby, Cellular Solids: Structure and Properties, Cellular Solids: Structure and Properties, Cambridge University Press, 1997.
[18] N.A. Fleck, V.S. Deshpande, M.F. Ashby, Micro-architectured materials: past, present and future, Proc. R. Soc. A Math. Phys. Eng. Sci. 466 (2010) 2495–2516.
[19] A. du Plessis, S.M.J. Razavi, M. Benedetti, S. Murchio, M. Leary, M. Watson, D. Bhate, F. Berto, Properties and applications of additively manufactured metallic cellular materials: a review, Prog. Mater. Sci. 125 (2022) 100918.
[20] J.A. Shaw, D.S. Grummon, J. Foltz, Superelastic NiTi honeycombs: fabrication and experiments, Smart Mater. Struct. 16 (2007) S170–S178.
[21] C. Bonatti, Design and Large Deformation Response of Additively-Manufactured shell-lattices, Design and Large Deformation Response of Additively-Manufactured Shell-Lattices, Massachusetts Institute of Technology, 2019.
[22] O. Al-Ketan, R. Rowshan, R.K. Abu Al-Rub, Topology-mechanical property relationship of 3D printed strut, skeletal, and sheet based periodic metallic cellular materials, Addit. Manuf. 19 (2018) 167–183.
[23] O. Al-Ketan, R. Rezgui, R. Rowshan, H. Du, N.X. Fang, R.K. Abu Al-Rub, Microarchitected stretching-dominated mechanical metamaterials with minimal surface topologies, Adv. Eng. Mater. 20 (2018) 1–15.
[24] S.N. Khaderi, V.S. Deshpande, N.A. Fleck, The stiffness and strength of the gyroid lattice, Int. J. Solids Struct. 51 (2014) 3866–3877.
[25] B. Haghgouyan, C. Hayrettin, T. Baxevanis, I. Karaman, D.C. Lagoudas, Fracture toughness of NiTi–Towards establishing standard test methods for phase transforming materials, Acta Mater. 162 (2019) 226–238.
[26] S. Gollerthan, M.L. Young, A. Baruj, J. Frenzel, W.W. Schmahl, G. Eggeler, Fracture mechanics and microstructure in NiTi shape memory alloys, Acta Mater. 57 (2009) 1015–1025.
[27] Y. Cui, X. Zeng, V.B.C. Tan, Z. Zhang, Experimental and numerical studies of NiTi dynamic fracture behaviors under the impact loading, Int. J. Mech. Sci. 235 (2022) 107724.
[28] A.L. McKelvey, Fatigue-crack propagation behavior in the shape-memory and superelastic alloy nitinol, Metall. Mater. Trans. A 32A (1999) 2001–2743.
[29] T. Tancogne-Dejean, A.B. Spierings, D. Mohr, Additively-manufactured metallic micro-lattice materials for high specific energy absorption under static and dynamic loading, Acta Mater. 116 (2016) 14–28.
[30] O. Al-Ketan, R.K. Abu Al-Rub, Multifunctional mechanical metamaterials based on triply periodic minimal surface lattices, Adv. Eng. Mater. 21 (2019) 1–39.
[31] N. Qiu, Y. Wan, Y. Shen, J. Fang, Experimental and numerical studies on mechanical properties of TPMS structures, Int. J. Mech. Sci. 261 (2024) 108657.
[32] F. Auricchio, R.L. Taylor, J. Lubliner, Shape-memory alloys: macromodelling and numerical simulations of the superelastic behavior, Comput. Methods Appl. Mech. Eng. 146 (1997) 281–312.
[33] F. Auricchio, R.L. Taylor, Shape-memory alloys: modelling and numerical simulations of the finite-strain superelastic behavior, Comput. Methods Appl. Mech. Eng. 143 (1997) 175–194.
[34] J.N. Zhu, E. Borisov, X. Liang, E. Farber, M.J.M. Hermans, V.A. Popovich, Predictive analytical modelling and experimental validation of processing maps in additive manufacturing of nitinol alloys, Addit. Manuf. 38 (2021) 101802.
[35] T. Maconachie, M. Leary, B. Lozanovski, X. Zhang, M. Qian, O. Faruque, M. Brandt, SLM lattice structures: properties, performance, applications and challenges, Mater. Des. 183 (2019) 108137.
[36] M. Benedetti, A. du Plessis, R.O. Ritchie, M. Dallago, S.M.J. Razavi, F. Berto, Architected cellular materials: a review on their mechanical properties towards fatigue-tolerant design and fabrication, Mater. Sci. Eng. R Rep. 144 (2021) 100606.
[37] S. Saedi, N. Shayesteh Moghaddam, A. Amerinatanzi, M. Elahinia, H.E. Karaca, On the effects of selective laser melting process parameters on microstructure and thermomechanical response of Ni-rich NiTi, Acta Mater. 144 (2018) 552–560.

[38] N. Shayesteh Moghaddam, S. Saedi, A. Amerinatanzi, A. Hinojos, A. Ramazani, J. Kundin, M.J. Mills, H. Karaca, M. Elahinia, Achieving superelasticity in additively manufactured NiTi in compression without post-process heat treatment, Sci. Rep. 9 (2019) 1–11.
[39] D. Han, X. Ren, Y. Zhang, X. Yu, X. Gang, C. Luo, Y. Min, Lightweight auxetic metamaterials : design and characteristic study, Compos. Struct. 293 (2022) 115706.
[40] S. Zhong, L. Zhang, Y. Li, X. Chen, S. Chai, G. Li, H. Liu, C. Guo, X. Wang, D. Zhang, J. Lu, Superelastic and robust NiTi alloys with hierarchical microstructures by laser powder bed fusion, Addit. Manuf. 90 (2024) 104319.
[41] H.Z. Lu, H.W. Ma, W.S. Cai, X. Luo, Z. Wang, C.H. Song, S. Yin, C. Yang, Stable tensile recovery strain induced by a Ni4Ti3 nanoprecipitate in a Ni50.4Ti49.6 shape memory alloy fabricated via selective laser melting, Acta Mater. 219 (2021) 117261.
[42] S.V. Harren, H.E. Dève, R.J. Asaro, Shear band formation in plane strain compression, Acta Metall. 36 (1988) 2435–2480.
[43] H. Vashishtha, P. Jamshidi, A. Vrettou, A. Kareer, M. Goode, H. Deyhle, A. James, S. Ahmad, C. Reinhard, M.M. Attallah, D.M. Collins, Microscale stress-geometry interactions in an additively manufactured NiTi cardiovascular stent: a synchrotron dual imaging tomography and diffraction study, Mater. Charact. 213 (2024) 114016.
[44] H. Sehitoglu, I. Karaman, R. Anderson, X. Zhang, K. Gall, H.J. Maier, Y. Chumlyakov, Compressive response of NiTi single crystals, Acta Mater. 48 (2000) 3311–3326.
[45] Y. Cao, X. Zhou, D. Cong, H. Zheng, Y. Cao, Z. Nie, Z. Chen, S. Li, N. Xu, Z. Gao, W. Cai, Y. Wang, Large tunable elastocaloric effect in additively manufactured Ni–Ti shape memory alloys, Acta Mater. 194 (2020) 178–189.